



Application of a chitosan bimetallic nanocomposite for the simultaneous removal of cadmium, nickel, and lead from aqueous solution

Charlton van der Horst^a, Bongiwe Silwana^a, Martin Makombe^a, Emmanuel Iwuoha^b, Vernon Somerset^{a,*}

^aDepartment of Chemistry, Faculty of Applied Sciences, Cape Peninsula University of Technology, Bellville 7535, South Africa, Mobile No. +27-73-2701789; Fax: +27-86-6631789; email: vsomerset@gmail.com/somersetv@cput.ac.za (V. Somerset), vanderhorstch@cput.ac.za (C. van der Horst), bsilwana@yahoo.com (B. Silwana), martin@scientificservices.co.za (M. Makombe)

^bSensorLab, Department of Chemistry, University of the Western Cape, Bellville 7535, South Africa, email: eiwuoha@uwc.ac.za

Received 11 June 2020; Accepted 5 December 2020

ABSTRACT

Wastewaters often consist of heavy metals and the use of iron-based bimetallic nanocomposites to remove these inorganic pollutants is still unclear. This investigation used a chitosan-iron/silver bimetallic nanocomposites (CS-Fe/AgNPs) to eliminate cadmium (Cd^{2+}), nickel (Ni^{2+}), and lead (Pb^{2+}) from aqueous solution. The chemically synthesized CS-Fe/AgNPs were characterized by scanning electron microscopy, transmission electron microscopy, Fourier transformed infrared spectroscopy, ultraviolet-visible spectroscopy, X-ray diffraction, and thermogravimetric analysis, which confirmed the shape, size, and composition of the bimetallic nanocomposite synthesized. The kinetics, adsorption isotherms, and thermodynamics of Cd^{2+} , Pb^{2+} , and Ni^{2+} were also studied in batch experiments. Analysis of inductively coupled plasma-optical emission spectroscopy was employed to quantify the amount of Cd^{2+} , Pb^{2+} , and Ni^{2+} absorbed by the CS-Fe/AgNPs from an aqueous solution. The results obtained revealed that Pb^{2+} , Cd^{2+} , and Ni^{2+} adsorption capacities using CS-Fe/AgNPs under optimized conditions were 2.01 mg g^{-1} for Pb^{2+} , 1.73 mg g^{-1} for Cd^{2+} , and 1.81 mg g^{-1} for Ni^{2+} , respectively. These results showed that the application of CS-Fe/Ag bimetallic nanocomposite can be applied to remove these heavy metals from wastewaters, simultaneously under optimized conditions such as effects of pH, contact time, and adsorbent dosage.

Keywords: Simultaneous adsorption; Heavy metals; Chitosan-iron/silver bimetallic nanocomposites; Nanoparticles

1. Introduction

Nowadays, especially in this century water has become the most important concern, so we need to preserve and guarantee this natural precious capital because it is our common future [1]. Large scale pollution caused by agricultural, domestic, and industrial activities decreases the supply of good quality water. Heavy metal pollution poses a prospective risk to aquatic and human health by their non-biodegradability, which are harmful at remarkably low

concentrations and widespread existence in anthropogenic and natural environments [2–4]. Anthropogenic activities such as pesticide development, metal industries, nickel-cadmium batteries manufacturing, plastics manufacturing, polymer production, pigment industries, electroplating, erosion, volcanic activity, electronics, photography, alloys, fertilizers, refining, and nuclear plants are the major sources of heavy metals into the environment [5,6].

Exposure to transition metal ions such as cadmium (Cd^{2+}), lead (Pb^{2+}), and nickel (Ni^{2+}) even at low levels can

* Corresponding author.

damage multiple organs in living organisms [7]. It has been demonstrated that Cd^{2+} can cause acute and chronic effects in humans such as kidney damage, psychological disorders, central nervous system damage, lung cancer, and prostate cancer [8,9]. The Environmental Protection Agency (EPA) [10] and World Health Organization (WHO) [11] have set a maximum limit in drinking water for Cd^{2+} to be 0.005 and 0.003 mg L^{-1} for cadmium, respectively. Lead has continuous toxicity, which can cause neurological, immunological, and cardiovascular diseases [12,13]. So for lead, the permissible limit is 0.010 mg L^{-1} in drinking water [14]. In the case of Ni^{2+} , it can also cause major harmful effects in humans such as kidney, lung, and cardiovascular diseases [15,16].

However, in recent years, various water treatment technologies, such as adsorption, coagulation, dialysis, membrane processes, osmosis, foam flotation, and biological photocatalytic degradation methods have been employed for the elimination of heavy metal ions from water and wastewaters [17,18]. Unfortunately, these methods have some drawbacks such as expensive instrumentation, high maintenance and operational cost, high energy condition, generation of sludge that contains toxic residual metals, and inadequate metal removal [19]. These drawbacks have encouraged scientists to develop alternative water treatment technologies that are less expensive and highly efficient for the elimination of heavy metals. In this regard, adsorption offers high efficiency, is less expensive, easy to handle, and metals recovery and other adsorbed species [20].

In previous studies, some effective adsorbents used to eliminate Pb^{2+} , Cd^{2+} , and Ni^{2+} ions are biopolymers [21], modified carbon [22], clays [23], zeolites [19], and bimetallic nanoparticles [18]. Among the different adsorbents, bimetallic nanoparticles are of greater interest from both Scientific and Technological views. Owing to their large surface area, improved electronic, optical, thermal, and catalytic performances [24], bimetallic nanoparticles are the most promising sorbents for heavy metal removal.

According to the literature, nanoscale zero-valent iron (nZVI) has been intensively used to eliminate heavy metals [25–27], organic compounds [28], and pesticides [29,30] in the environment. For example, Geng et al. [31] used Fe^0 nanoparticles that were stabilized by chitosan (CS) for the elimination of Cr^{6+} in water. Liu et al. [32] removed heavy metals from wastewater produced by the electroplating industry using enhanced CS beads-supported Fe^0 nanoparticles. Unfortunately, the stability of nZVI is poor and it tends to agglomerate easily [33], so the ability to reduce pollutants is decreased. In this regard, researchers have loaded alternative metal such as Au, Ni, Pd, Pt, and Ag, on the surface of nZVI to increase the performance and accelerate the reduction rate [34–36]. Among various elements, silver nanoparticles have high electrochemical potential and have been used to increase the catalytic ability of nZVI [37]. Many scientists [38] have synthesized Ag-based bimetallic nanoparticles such as Bi-Ag [39], Ag-ZnO [40], Ag/Fe [41], and Ag@Pt [42] for environmental applications.

These bimetallic nanoparticles tend to aggregate together to be more stable due to the high energy level of surface state and van der Waals attraction. This aggregation of bimetallic nanoparticles can be reduced by applying

a supporting matrix with functional groups [18,40,41] or organic surfactants [43,44]. For example, Wu and Feng [41] used biochar to stabilize Ag/FeNPs. Kakavandi et al. [45] used activated carbon with nZVI and Ag bimetallic nanoparticles for enhancing the elimination of Cr^{6+} . In this investigation, the focus was shifted and CS was used because it's an amino polymer, a derivative of chitin, a naturally occurring biopolymer which is the second most abundant polysaccharide in the world, after cellulose [46]. Due to the high contents of amino, its low cost, and hydroxyl functional groups compared to other polymers, CS displaying high adsorption potential for several aquatic contaminants and has drawn particular attention as an effective biosorbent [47,48]. The major application of chitosan is based on its ability to tightly bind contaminants, in particular, ions of heavy metals. To the best of our knowledge, there is still no investigation previously reported about Fe/AgNPs impregnated into CS for the elimination of heavy metal ions from aqueous solutions.

In this investigation, the main objectives were therefore to synthesize CS-Fe/AgNPs and to do characterization on the surface properties of this CS-Fe/AgNPs by comparing them with chitosan and Fe/AgNPs individually, and to determine the surface structure and chemical functional groups responsible for the adsorption of heavy metals using X-ray diffraction (XRD), transmission electron microscopy (TEM), scanning electron microscopy (SEM), ultraviolet-visible spectroscopy (UV-Vis), and Fourier transformed infrared spectroscopy (FT-IR) techniques for chemical and morphological structure elucidation. The other objective was to optimize the parameters for simultaneous adsorption such as contact time, adsorbent dosage, pH, and study thermodynamics, equilibrium constants, and kinetics of the simultaneous adsorption of Cd^{2+} , Pb^{2+} , and Ni^{2+} ions from aqueous solutions.

2. Materials and methods

2.1. Reagents

Chitosan (CS) and sodium borohydride (NaBH_4) used in this experiment were supplied by Sigma-Aldrich (Germany). Iron chloride hexahydrate ($\text{FeCl}_3 \cdot 6\text{H}_2\text{O}$) and silver nitrate (AgNO_3) were procured from Educhem (South Africa). Ethanol ($\text{CH}_3\text{CH}_2\text{OH}$), sodium hydroxide (NaOH), and acetic acid were procured from Kimix, chemical, and laboratory suppliers (South Africa). The heavy metal standards (1,000 mg L^{-1} AAS) that were used in this study were all procured from Fluka (South Africa). All solutions were prepared using Milli-Q (18.2 M Ω ; Millipore systems) deionized water.

2.2. Fe/Ag bimetallic nanoparticles preparation

Iron silver bimetallic nanoparticles (Fe/AgNPs) were prepared by a reduction procedure described by Yuvakkumar et al. [48] with some modification using $\text{FeCl}_3 \cdot 6\text{H}_2\text{O}$, AgNO_3 , and NaBH_4 in ambient pressure, room temperature, and aerobic conditions. Approximately, 0.5 g solution of $\text{FeCl}_3 \cdot 6\text{H}_2\text{O}$ and 1.8 g AgNO_3 were prepared separately in a 1:4 (v/v) water:ethanol mixture (10 mL deionized water

and 40 mL ethanol) and agitated well. A 0.1 M NaBH₄ solution was prepared by dissolving 0.3 g of NaBH₄ in 100 mL of Milli-Q deionized water. To start the procedure, the NaBH₄ solution was added to the solutions of FeCl₃·6H₂O and AgNO₃ with continuous stirring. After the first drop of NaBH₄ solution, solid gray nanoparticles instantly appeared, and then the remaining NaBH₄ was added for the completion of the reduction reaction. The mixture was left for additional 10 min of stirring after the addition of the remaining NaBH₄ solution. The reduction reaction products were washed numerous times using absolute ethanol and a Buchner funnel to eliminate all the water. The end product was dried overnight in an oven at 323 K. Dry polyethylene flask was employed to transfer the dried Fe/AgNPs and were preserved with a thin layer of ethanol to prevent that the Fe/AgNPs from oxidation. The resulting product was collected, stored, and prepared for characterization.

2.3. Preparation of CS-Fe/Ag bimetallic nanocomposite

Chitosan-iron/silver bimetallic nanocomposite (CS-Fe/AgNP) was prepared according to the procedure described elsewhere in the literature [32,49]. Approximately, 2.0 g chitosan (CS) flakes were dissolved in 100 mL 5.0% (v/v) acetic acid solution for 24 h with continuous stirring until complete dissolution. After continuous stirring of 24 h, a 1.0 g amount of Fe/AgNPs were slowly added into the CS polymer solution. The CS-Fe/AgNPs mixture was quickly dropped into a 2 mol L⁻¹ NaOH solution to form CS-Fe/AgNPs. The nanocomposite remained in a solution of NaOH for 1 d to get harder and then was washed with pure Milli-Q deionized water. The CS-Fe/AgNPs were stored for further use in deionized water.

2.4. Analytical methods

A SEM was employed to investigate the surface morphologies (SEM, ZEISS, Germany) [50]. TEM was employed to record the images of the synthesized materials (TEM, Oregon, USA). FT-IR spectra of prepared CS, Fe/AgNPs, and CS-Fe/AgNPs were obtained using a Bruker Alpha-T, infrared spectrometer (Bruker, South Africa). UV-Vis spectroscopic analysis was obtained using a ThermoFisher Spectronic Helios spectrometer (Thermo, USA) [38,50]. The XRD patterns of CS, Fe/AgNPs, and CS-Fe/AgNPs were investigated by a Philips-X'Pert Pro MPD instrument (Philips, Netherlands) [18]. Thermogravimetric analysis (TGA) was performed by using the TGA Q500 instrument (ELTRA's TGA Thermostep, Germany).

2.5. Batch experiments

Batch experiments were performed to eliminate of Cd²⁺, Pb²⁺, and Ni²⁺ ions simultaneously by CS-Fe/AgNPs in 100 mL Erlenmeyer flasks. In these batch experiments, 1 g of CS-Fe/AgNPs were added followed by the addition of Cd²⁺, Pb²⁺, and Ni²⁺ ions 25 mL solutions with known concentrations. The mixture was agitated for 120 min at 100 rpm in a room with a constant temperature. After this agitation time, the CS-Fe/AgNPs was centrifuge to separate it from the model solution by filtration, and the concentrations of

Cd²⁺, Pb²⁺, and Ni²⁺ ions were determined simultaneously in the filtrate. The effects of initial heavy metal ions concentration (5–60 mg L⁻¹), contact time (60–360 min), pH (3–8.5), and adsorbent dosage (0.25–2.5 g L⁻¹) were also investigated. In the case of isotherm studies, various concentrations of metal ions were used at optimum pH value, constant contact time, and adsorbent dosage. These experiments were conducted in triplicate and their average was reported. The concentration of Pb²⁺, Cd²⁺, and Ni²⁺ ions in model solutions was measured by an inductively coupled atomic emission spectrometer (ICP-AES) Thermo Scientific® iCAP 6200 (Barrington, USA) [51].

The individual uptake capacity (q) of Pb²⁺, Cd²⁺, and Ni²⁺ ions using CS-Fe/AgNPs were calculated using Eq. (1) [40,49].

$$q_e = \frac{(C_0 - C_t)}{W} \times V \quad (1)$$

where q_e (mg g⁻¹) is the quantity adsorbed per gram of adsorbent at time t (min), C_0 (mg L⁻¹) represents the initial concentration of heavy metals in the model solution and C_t (mg L⁻¹) represents the concentration of heavy metals at t min, W (g) is the mass of the adsorbents, and V (L) is the volume of heavy metals solutions.

3. Results and discussions

3.1. Morphology

The SEM images of Fe/AgNPs and CS-Fe/AgNPs are illustrated in Figs. 1a and b, respectively. In Fig. 1a, the shape of the Fe/AgNPs was found to be sphere-shaped, with a diameter of approximately 10–50 nm and accompanied by some chain-like aggregates. Fig. 1b illustrates the SEM image of CS-Fe/AgNPs that is also spherical in shape with both Fe/AgNPs and CS polymers aligned on top of each other. The CS-Fe/AgNPs has a diameter of approximately 10–120 nm.

Both the shape and particle size of Fe/AgNPs and CS-Fe/AgNPs were analyzed by TEM and illustrated in Figs. 1c and d, respectively. Fig. 1 shows that Fe/AgNPs are spherical in shape, with chain-like aggregates, that are 20–80 nm in diameter. Fig. 1d shows that Fe/AgNPs and CS polymers are both spherical in shape with Fe/AgNPs aligned on top of CS polymers. The CS-Fe/AgNPs has a diameter of 5–10 nm.

3.2. FT-IR and UV-Vis analysis

UV-Vis spectrum of CS, Fe/AgNPs, and CS-Fe/AgNPs is illustrated in Fig. 2a. The UV-Vis experiments were conducted over a range of 190–1,000 nm. In Fig. 2a, no absorbance peak was detected for the solution comprising dissolved unmodified CS. In the case of Fe/AgNPs, two characteristic absorption peaks were observed at wavelengths of 300 and 380 nm, which confirmed the formation of iron and silver nanoparticles. The broad featureless absorption peak at 300 nm falls in the bandgap of semiconductor materials [52]. The UV-Vis spectrum of CS-Fe/AgNPs also features two absorption peaks at wavelengths

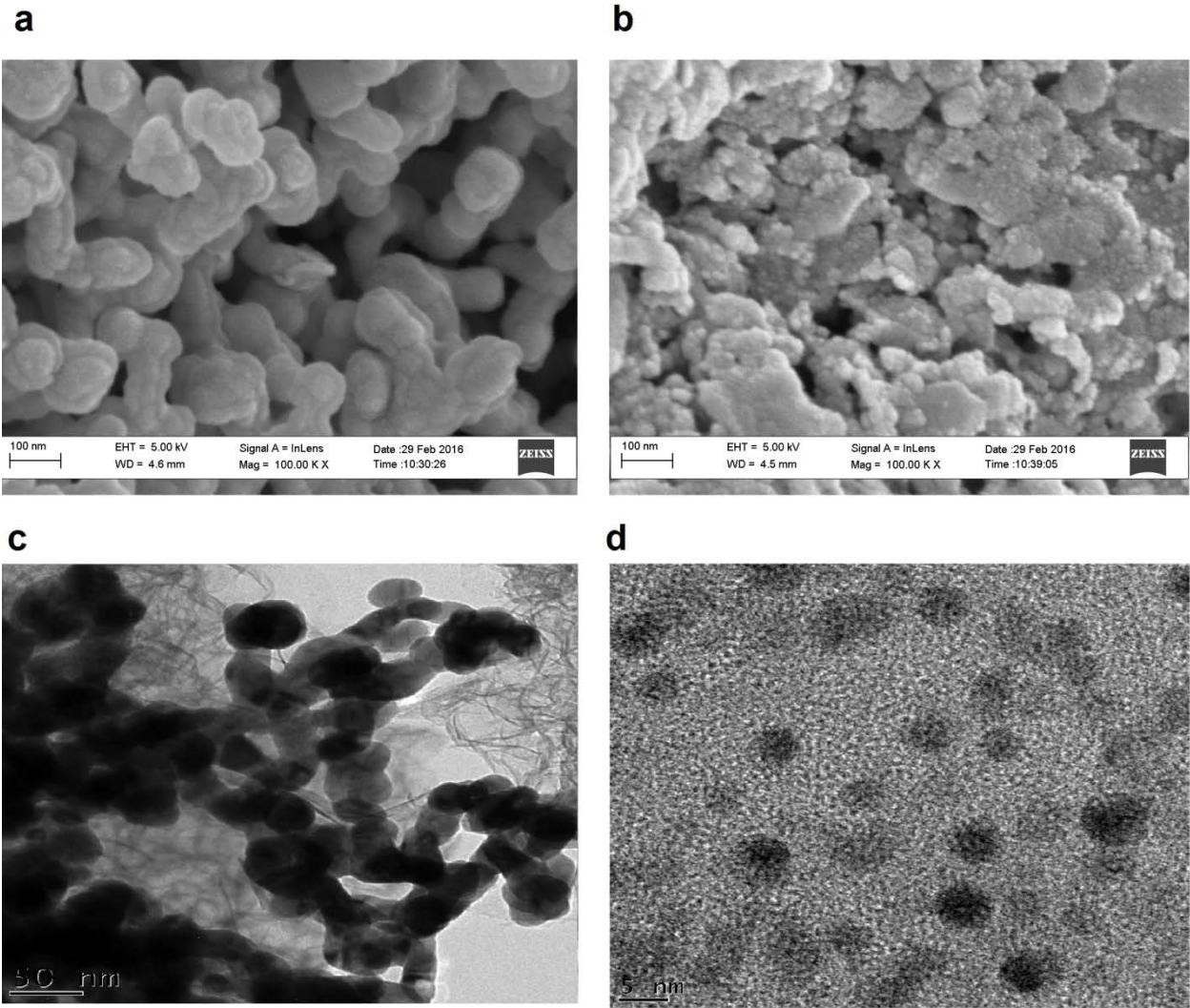


Fig. 1. SEM images of (a) Fe/AgNPs and (b) CS-Fe/AgNPs. TEM images of (c) Fe/AgNPs and (d) CS-Fe/AgNPs.

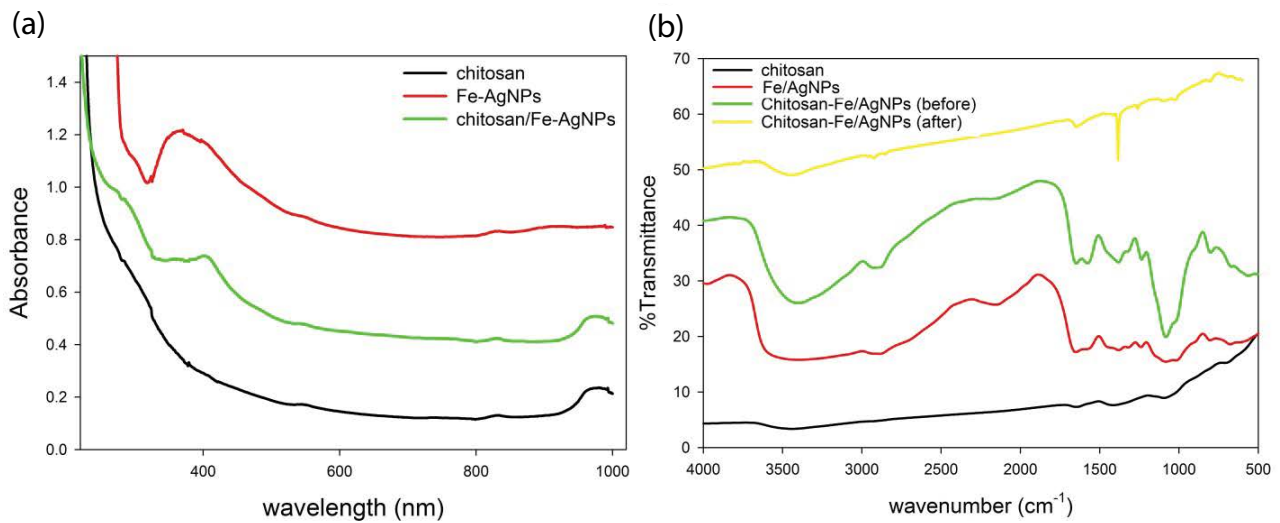


Fig. 2. UV-Vis spectra of (a) for CS, Fe/AgNPs, and CS-Fe/AgNPs. FTIR spectra of (b) for CS, Fe/AgNPs, and CS-Fe/AgNPs before adsorption and CS-Fe/AgNPs after adsorption.

of 300 and 400 nm. A slight shift in wavelength for the silver absorbance peak was observed.

Molecular motion and fingerprinting of the synthesized materials were assessed by FT-IR spectroscopy. Fig. 2b shows FT-IR spectra for Fe/AgNPs, CS, and CS-Fe/AgNPs, respectively. The FT-IR spectrum of CS showed results for the C–O–C band stretching around $1,110\text{ cm}^{-1}$, N–H angular distortion in the CO–NH plane at $1,531\text{ cm}^{-1}$, C–H and C–N stretching at $2,930\text{ cm}^{-1}$, and O–H stretching at $3,455\text{ cm}^{-1}$ that relates well with the results reported in the literature [53,54]. For the Fe/AgNPs, the bands observed at $1,100$ and $1,360\text{ cm}^{-1}$ in the spectrum can be ascribed to the ethanol used in the preparation procedure of the sample. Compared to the FT-IR spectra of CS, there are changes in bands from CS-Fe/AgNPs where the N–H and O–H band shifts from higher wavenumber to lower wavenumber. The decrease in wavenumber illustrates the effect of the Fe/AgNPs interaction with these functional groups on the CS structure. In the CS-Fe/AgNPs spectrum, a new peak at 580 cm^{-1} was observed, which is an indication that the Fe–O group, so it demonstrates that iron was successfully deposited on the CS. The structure of CS contains functional groups such as the N–H group and the O–H group and they act as electron donors. The N–H group and the O–H group participate in electrostatic interactions and are used for the stabilization of CS-Fe/AgNPs [55].

In Fig. 2b, the FT-IR spectra have shown a significant difference between the CS-Fe/AgNPs before and after adsorption. In adsorption studies, it is important to identify what interaction occurring at the adsorbent and adsorbate interface. The heavy metals adsorption onto the surface of the CS-Fe/AgNPs occurs through chelation and ion-exchange between the ionized functional groups within the adsorbent and positively charged heavy metal ions. The FT-IR spectra in Fig. 2b for before and after adsorption of heavy metal ions confirms this interaction. After the adsorption process, the –NH group peak intensity in amine decreased, this is due that N_2 atoms act as the main sites for heavy metals adsorption on the CS-Fe/AgNPs. The peak at $1,650\text{ cm}^{-1}$ after adsorption is the formation of metal chelate with N_2 atoms in the amino groups. The strong peak at $3,455\text{ cm}^{-1}$ relates to OH-groups and the shift to $3,435\text{ cm}^{-1}$ is an indication that –OH groups positively influence the adsorption process. Some of the peaks have broadened with a slight shifting in wavenumber indicating that the functional groups present in CS-Fe/AgNPs had interacted with the heavy metals in the solution. The obtained results are similar to the results of previous studies [56].

3.3. XRD and TG analysis

The structural properties of the synthesized CS, Fe/AgNPs, and CS-Fe/AgNPs were further studied using XRD techniques. The XRD spectrum for CS in Fig. 3a shows two characteristic 2θ peaks between 17° and 20° . The two peaks for CS match well with the literature values [57–59]. The enlargement of the peaks for CS can be attributed to the amorphous nature of the biopolymer [60]. In Fig. 3a, the XRD spectrum of the Fe/AgNPs shows three characteristic peaks around 38.06° (main peak), 44.66° , and 64.34° that corresponds to the Ag-111, Fe-110, and Fe-200 diffraction

peaks, respectively [61,62]. The XRD pattern obtained for CS-Fe/AgNPs illustrates peaks of both CS and Fe/AgNPs. The values obtained for this nanocomposite agreed well with the individual values obtained above for both CS and Fe/Ag bimetallic nanoparticles.

TGA was employed to determine the mass percentage of each of the CS, Fe/AgNPs, and CS-Fe/AgNPs and illustrated in Fig. 3b. The TGA pattern for Fe/AgNPs indicates that there was a small weight loss from 25°C to 680°C intervals. For CS, the TGA results show that from 25°C to 130°C the mass loss of the biopolymer was relatively small (7%) because of the elimination of absorbed physical and chemical water. The principle chains of CS began to degrade at approximately 160°C – 360°C and the temperature of the final breakdown was around 380°C – 680°C , with significant mass loss (68%). According to Wang et al. [63], the second and third mass loss for chitosan could be attributed to the breakdown of etheral groups and the breakdown of glucosamine residues, respectively.

3.4. Batch experiments

3.4.1. Effect of pH

The solution pH and contact time are two of the greatest important parameters which could affect the removal process of Cd^{2+} , Pb^{2+} , and Ni^{2+} ions [64]. Fig. 4a illustrates the effect of pH on the adsorption of Cd^{2+} , Pb^{2+} , and Ni^{2+} ions over a pH range between 3 and up to 8.5. The results showed little adsorption of heavy metal ions at pH 3 due to hydrogen ions competing with these heavy metal ions for adsorption sites [65]. Maximum adsorption was obtained at pH 4.36 and recorded as the optimum pH. The adsorption decreased slowly from pH 5 up to pH 8.5 owing to the precipitation of the metal ions as hydroxides which reduced the speed of adsorption and further reduced the removal percentage of these heavy metal ions [65]. The adsorption of positively charged metal ions such as Cd^{2+} , Pb^{2+} , and Ni^{2+} increases the attraction of electrostatic interactions between the positive heavy metal ions and the surface of the CS-Fe/AgNPs adsorbent. These observations of the pH effect have been observed in other studies reported in the literature [66].

3.4.2. Effect of contact time

The contact time effect on the Cd^{2+} , Pb^{2+} , and Ni^{2+} ions adsorption is illustrated in Fig. 4b with the following experimental parameters: optimal pH (pH = 4.36), a 1.0 g L^{-1} adsorbent solution, and the contact time were evaluated at different time intervals from 1 to 6 h. The Pb^{2+} , Cd^{2+} , and Ni^{2+} ions adsorption capacities as indicated in Fig. 4b were increased from 1 up to 3 h and it remained constant from 4 to 6 h. In further experiments, the contact time of 4 h was used because it ensured the high removal of these heavy metals. Similar results have been found in the literature reported by other scientists [67].

3.4.3. Effect of adsorbent dosage

Adsorbent dosage plays always an important part in the adsorption of heavy metal ions from wastewater samples.

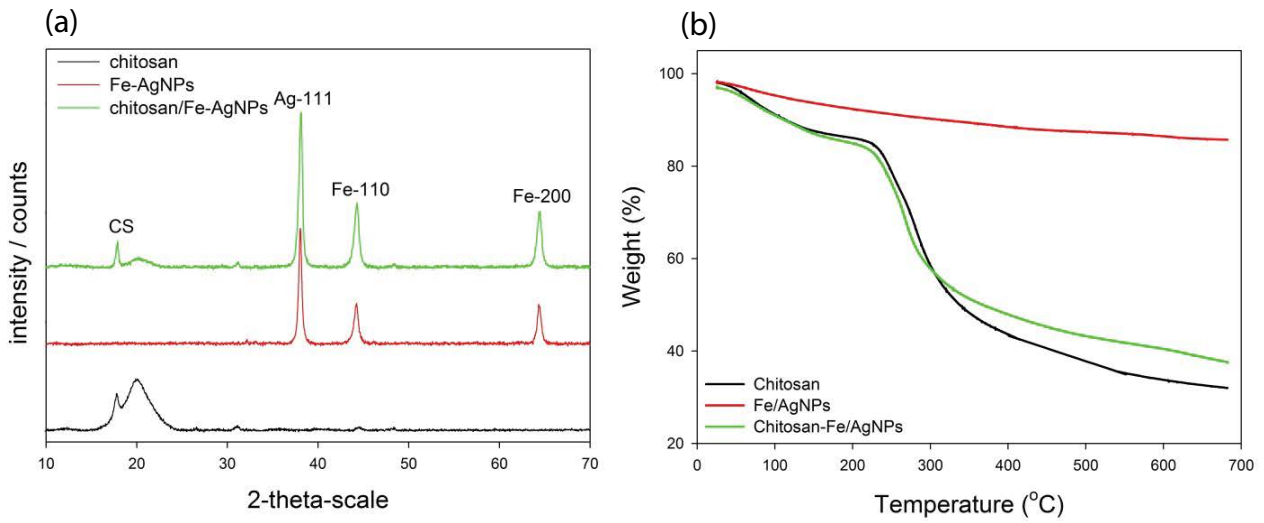


Fig. 3. XRD pattern of (a) for CS, Fe/AgNPs, and CS-Fe/AgNPs. TGA spectra of (b) for CS, Fe/AgNPs, and CS-Fe/AgNPs.

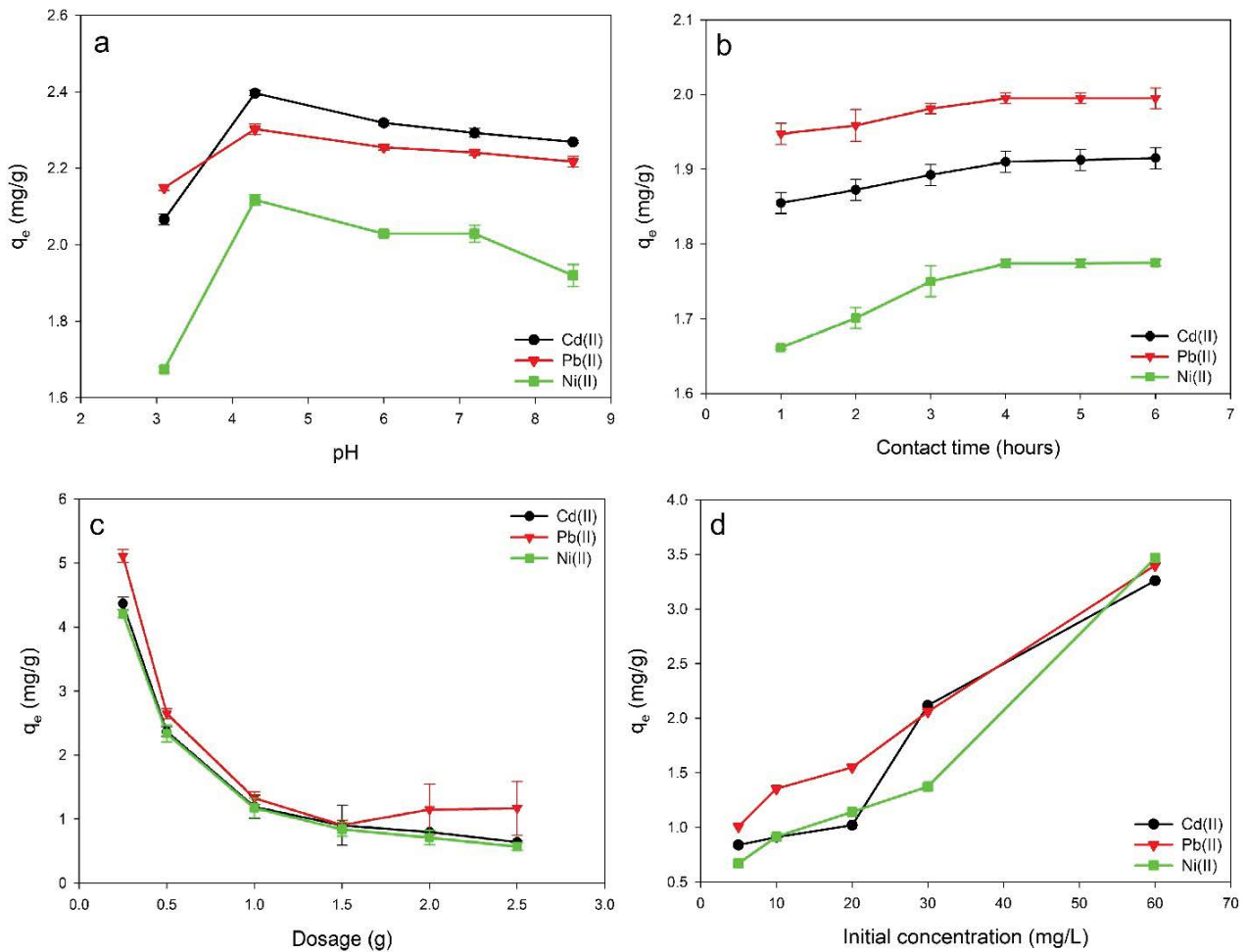


Fig. 4. Results for the effect of pH (a), contact time (b), adsorbent dosage (c), and initial concentration (d) on the adsorption of Cd²⁺, Pb²⁺, and Ni²⁺ onto CS-Fe/AgNPs.

In the present investigation, at room temperature, the concentration of the adsorbent dosage that was used ranged from 0.25 to 2.5 g L⁻¹. The results in Fig. 4c show that the removal efficiency becomes greater as the concentration of the adsorbent dosage was increased. This observation is due to large surface area and active adsorption sites on the CS-Fe/AgNPs [68]. In Fig. 4c, the adsorption capacity of CS-Fe/AgNPs becomes smaller with an increase in adsorbent dosage. This observation may be a result of heavy metals aggregation at the surface of the adsorbent and the diffusion path length might be increased [44]. This observation of the adsorbent dosage effect has been observed in other studies reported in the literature [25].

3.4.4. Effect of initial concentration

The initial concentration effect is also an important parameter in the study of the equilibrium adsorption of the CS-Fe/AgNPs adsorbent. The initial concentration of the heavy metal ions is used to overcome the mass-transfer barrier between the CS-Fe/AgNPs adsorbent and adsorbate medium. In the study of the initial concentration effect, different concentrations of heavy metal ions (from 5 to 60 mg L⁻¹) were used at optimum pH value, constant adsorbent dosage, and contact time. The results in Fig. 4d illustrates the initial concentration becomes greater as the concentration of the heavy metal ions was increased. This phenomenon is due to the availability of active sites on the adsorbent surface. Besides, at equilibrium, the heavy metal ions will not be adsorbed onto the active sites of the adsorbent anymore. Similar observations had been found in some other investigation reported elsewhere in the literature [69].

3.5. Adsorption kinetics

The experimental data obtained for the removal process of Cd²⁺, Pb²⁺, and Ni²⁺ ions onto CS-Fe/Ag bimetallic nanocomposite were fit into the pseudo-first-order and the pseudo-second-order kinetic models. Below is the equation for the pseudo-first-order equation and are illustrated as [70]:

$$\log(q_e - q_t) = \log q_e + \frac{k_1 t}{2.303} \quad (2)$$

where t is the reaction time, q_t is the concentration adsorbed at a specific interval (mg g⁻¹), q_e is the concentration adsorbed at (mg g⁻¹), k_1 is the pseudo-first-order model rate constant (g mg⁻¹ min⁻¹). For the pseudo-first-order model, q_e and k_1 values were obtained from the intercept and the linear regression slope of $\log(q_e - q_t)$ vs. t . The linear regression plots of the pseudo-first-order kinetic model and the pseudo-second-order kinetic model for Cd²⁺, Pb²⁺, and Ni²⁺ ions adsorption onto CS-Fe/AgNPs is illustrated in Fig. 5. According to Eq. (2), the values for k_1 and q_e were calculated for Cd²⁺, Pb²⁺, and Ni²⁺ ions, respectively, and illustrated in Table 1. The value for q_e calculated was lower than the experimental results. In Table 1, low correlation coefficients (R^2) for the three metal ions were observed. The pseudo-first-order model is not applicable to describe the kinetics of Cd²⁺, Pb²⁺, and Ni²⁺ ions by adsorption using CS-Fe/AgNPs as the adsorbents [71].

The pseudo-second-order equation was stated below by the following equation [72]:

$$\frac{t}{q_t} = \frac{1}{k_2 q_e^2} + \frac{t}{q_e} \quad (3)$$

where q_e is the adsorption capacity at adsorption equilibrium (mg g⁻¹), and q_t is the adsorption capacity at the specific time (mg g⁻¹), k_2 is the rate constant of the pseudo-second-order model (g mg⁻¹ min⁻¹) and can be calculated by the slope of the regression plot of t/q_t vs. t . From Eq. (3), k_2 and q_e were calculated for Cd²⁺, Pb²⁺, and Ni²⁺ ions, respectively, and illustrated in Table 1. The pseudo-second-order adsorption correlation coefficient (R^2) was better than 0.99 and showed good linearity. The correlation coefficient (R^2) results obtained for the pseudo-second-order adsorption model illustrates the chemisorption of Pb²⁺, Ni²⁺, and Cd²⁺ ions, onto CS-Fe/AgNPs [73].

3.6. Adsorption isotherms

In adsorption studies, the adsorption isotherm defines the adsorption capacity. According to the literature, various models such as Langmuir, Freundlich, Temkin, and Dubinin–Radushkevich have been developed to describe the behavior of the adsorbent materials [74]. The Langmuir isotherm theory is built on the assumption that adsorption is taking place on a homogenous and uniform surface of materials that forms a monolayer. Walker and Weatherley [75] stated that when adsorbate molecules formed a layer on the surface of the adsorbent, the adsorbent becomes saturated. The linear form of the Langmuir isotherm was employed to the data as the following equation:

$$\frac{1}{q_e} = \frac{1}{QbC_e} + \frac{1}{Q} \quad (4)$$

where q_e (mg g⁻¹) is the number of heavy metal ions adsorbed onto the CS-Fe/AgNPs, Q (mg g⁻¹) is the maximum adsorption capacity of the adsorbent for the heavy metals, C_e (mg L⁻¹) is the concentration of the heavy metal ions at equilibrium time in the solution, and b (L mg⁻¹) is the constant related to the net enthalpy of adsorption. The b and Q were determined from the slope and intercept of the linear plot of C_e/q_e vs. C_e in Fig. 6 and are illustrated in Table 2. Table 2 illustrates that the Langmuir maximum adsorption capacity of the CS-Fe/AgNPs was found to be 0.433, 0.922, and 1.909 mg g⁻¹ for Pb²⁺, Cd²⁺, and Ni²⁺ ions, respectively. From the observed results in Table 2, the R^2 values for this isotherm were found to be 0.6993, 0.4574, and 0.7840 for Pb²⁺, Cd²⁺, and Ni²⁺ ions, respectively. These values were not close enough to 1 and indicate that the Langmuir isotherm is not in good agreement with the investigational data.

The Freundlich isotherm theory is built on the assumption that adsorption takes place on heterogeneous surfaces and is appropriate for the monolayer adsorption (chemical adsorption) and the multilayer adsorption (physical adsorption) [76]. The Freundlich isotherm could be derived by using the following equation:

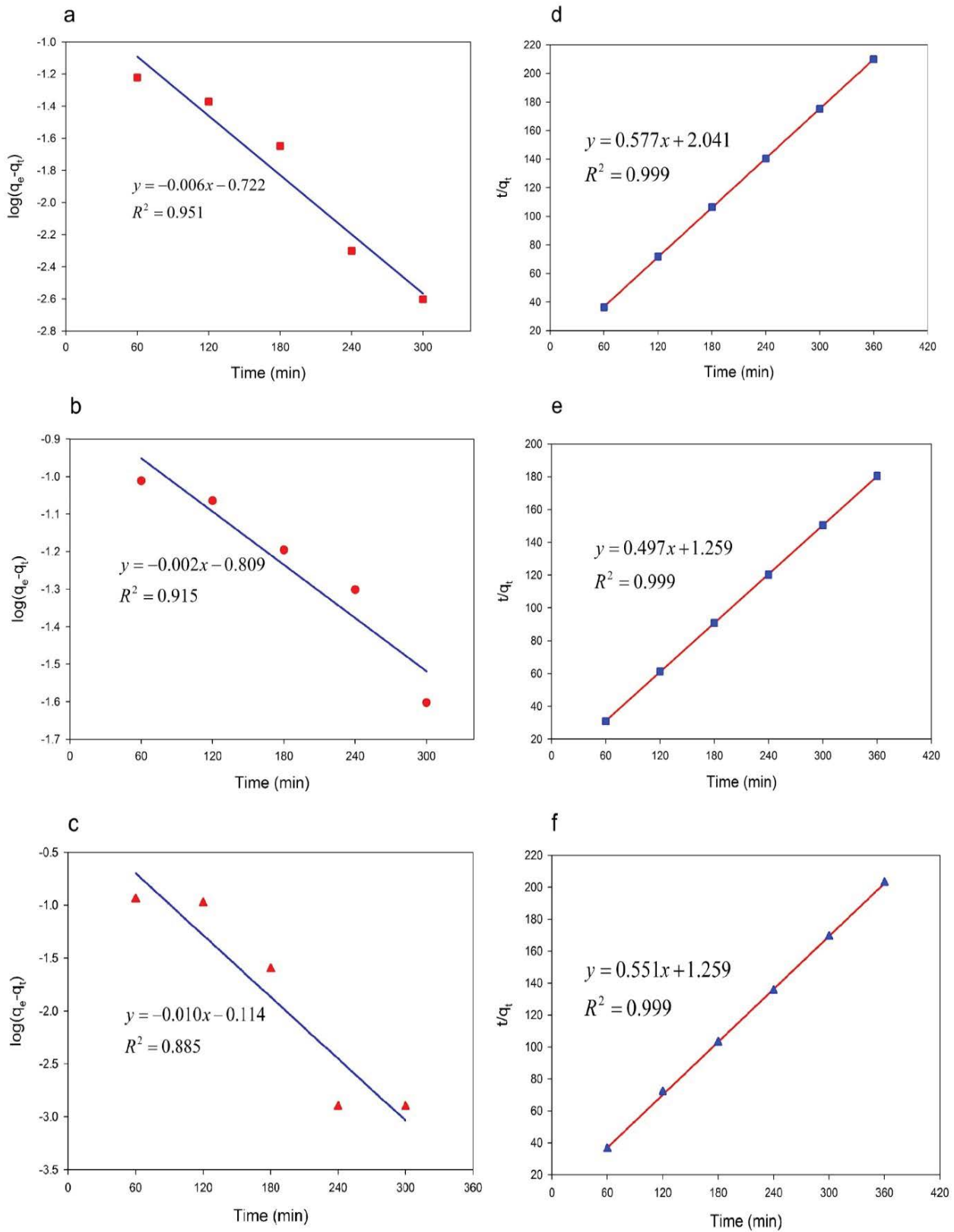


Fig. 5. Pseudo-first-order kinetic (a–c), pseudo-second-order kinetic (d–f) for adsorption of Cd^{2+} , Pb^{2+} , and Ni^{2+} ions onto CS-Fe/AgNPs.

Table 1
Kinetic model parameters for Cd²⁺, Pb²⁺, and Ni²⁺ ions adsorption using CS-Fe/AgNPs

Pollutant	Pseudo-first-order			Pseudo-second-order		
	$q_{e,exp}$ (mg g ⁻¹)	k_1 (min ⁻¹)	R^2	$q_{e,cal}$ (mg g ⁻¹)	k_2 (mg mg ⁻¹ min ⁻¹)	R^2
Cd ²⁺	0.189	0.014	0.9514	1.73	0.164	0.9999
Ni ²⁺	0.770	0.022	0.8848	1.81	0.078	0.9997
Pb ²⁺	0.155	0.0055	0.9152	2.01	0.197	0.9999

Table 2
Isotherm equation parameters for Pb²⁺, Ni²⁺, and Cd²⁺ adsorption using CS-Fe/AgNPs

Pollutant	Langmuir model				Freundlich model		
	q_m (mg g ⁻¹)	k_L (L mg ⁻¹)	R_L	R^2	k_f (mg g ⁻¹)	$1/n$	R^2
Cd ²⁺	0.922	1.77	0.102	0.4574	0.25	1.00	0.9999
Ni ²⁺	0.433	0.24	0.450	0.7840	0.26	1.03	0.9998
Pb ²⁺	1.909	1.10	0.150	0.6993	0.28	1.08	0.9978

$$\log q_e = K + \frac{1}{n} \log C_e \quad (5)$$

where q_e (mg g⁻¹) is the number of heavy metals adsorbed, C_e is the concentration of the heavy metals at equilibrium (mg L⁻¹), K can be taken as the adsorption coefficient, and n is the constant of Freundlich isotherm which illustrates the adsorption process favorability. The value of n should be between 1 and 10 for favorable adsorption conditions. Table 2 illustrates the results obtained from Freundlich isotherm analysis and shown that Cd²⁺, Pb²⁺, and Ni²⁺ ions were favorably adsorbed onto CS-Fe/AgNPs. The R^2 values of Cd²⁺, Pb²⁺, and Ni²⁺ ions for the Freundlich isotherm model in Table 2 ($R^2 > 0.99$) are close to 1 and indicate that the Freundlich isotherm is in good agreement with the investigational data.

3.7. Thermodynamic studies

The thermodynamic studies of heavy metal ions adsorbed onto CS-Fe/AgNPs were used to explore if the adsorption is exothermic or endothermic. The thermodynamic parameters such as entropy (ΔS°), enthalpy (ΔH°), and the standard free energy (ΔG°) were determined by applying the following equations [74,77].

$$K_c = \frac{q_e}{C_e} \quad (6)$$

$$\Delta G^\circ = -RT \ln K_c \quad (7)$$

$$\ln K_c = \frac{-\Delta H^\circ}{RT} + \frac{\Delta S^\circ}{R} \quad (8)$$

$$\Delta G^\circ = \Delta H^\circ - T \Delta S^\circ \quad (9)$$

where K_c (L mol⁻¹) is the standard thermodynamic equilibrium constant obtained by q_e/C_e , R (8.314 J mol⁻¹ K⁻¹) is

the gas constant, and T (K) is the absolute temperature. The standard free energy (ΔG°) was determined at each temperature employing Eq. (7). The values of entropy change (ΔS°) and enthalpy change (ΔH°) were determined from the slope and intercept of the Van't Hoff plot ($\ln K_c$ vs. $1/K$) in Fig. 7, respectively [78]. Table 3 illustrates the various thermodynamic parameters calculated for Cd²⁺, Pb²⁺, and Ni²⁺ at the three temperatures. The negative values of ΔG° at all temperatures for the adsorption process of Pb²⁺, Cd²⁺, and Ni²⁺ on CS-Fe/AgNPs active adsorption sites indicate a spontaneous process or reaction. The positive values of ΔH° in this study illustrate an endothermic adsorption process. The value of ΔS° for Pb²⁺, Cd²⁺, and Ni²⁺ was also positive, which illustrates that the adsorption efficiency increases in solid/liquid phases with an increase in temperature.

3.8. Reusability of the CS-Fe/Ag

The desorption study of CS-Fe/AgNPs is very important because the cost-effectiveness of the adsorption process is determined by the regeneration of the adsorbent [79]. The reuse value of the CS-Fe/AgNPs was done by using a 0.01 M solution of NaOH as the desorbing agent. This process is performed by triplicate the adsorption-desorption experiments. A slight difference in Pb²⁺, Cd²⁺, and Ni²⁺ adsorption capacity of CS-Fe/AgNPs was observed after one regeneration cycle. The Cd²⁺, Pb²⁺, and Ni²⁺ adsorption capacity from the initial desorption by the first cycle in Fig. 8 results in a regeneration efficiency of 92.2% for Pb²⁺, 82.7% for Cd²⁺, and 87.0% for Ni²⁺, respectively. In the case of the second cycle, a sharp decrease in the adsorption capacity was observed with a regeneration efficiency of 62.7% for Pb²⁺, 70.9% for Cd²⁺, and 74.6% for Ni²⁺, respectively. This phenomenon may be due to adsorbed heavy metals and at each cycle, some adsorption sites do not get free by the 0.01 M of NaOH desorbing solution and decrease the adsorption capacity of CS-Fe/AgNPs [80]. According to the regeneration results observed in this study, the results suggest the

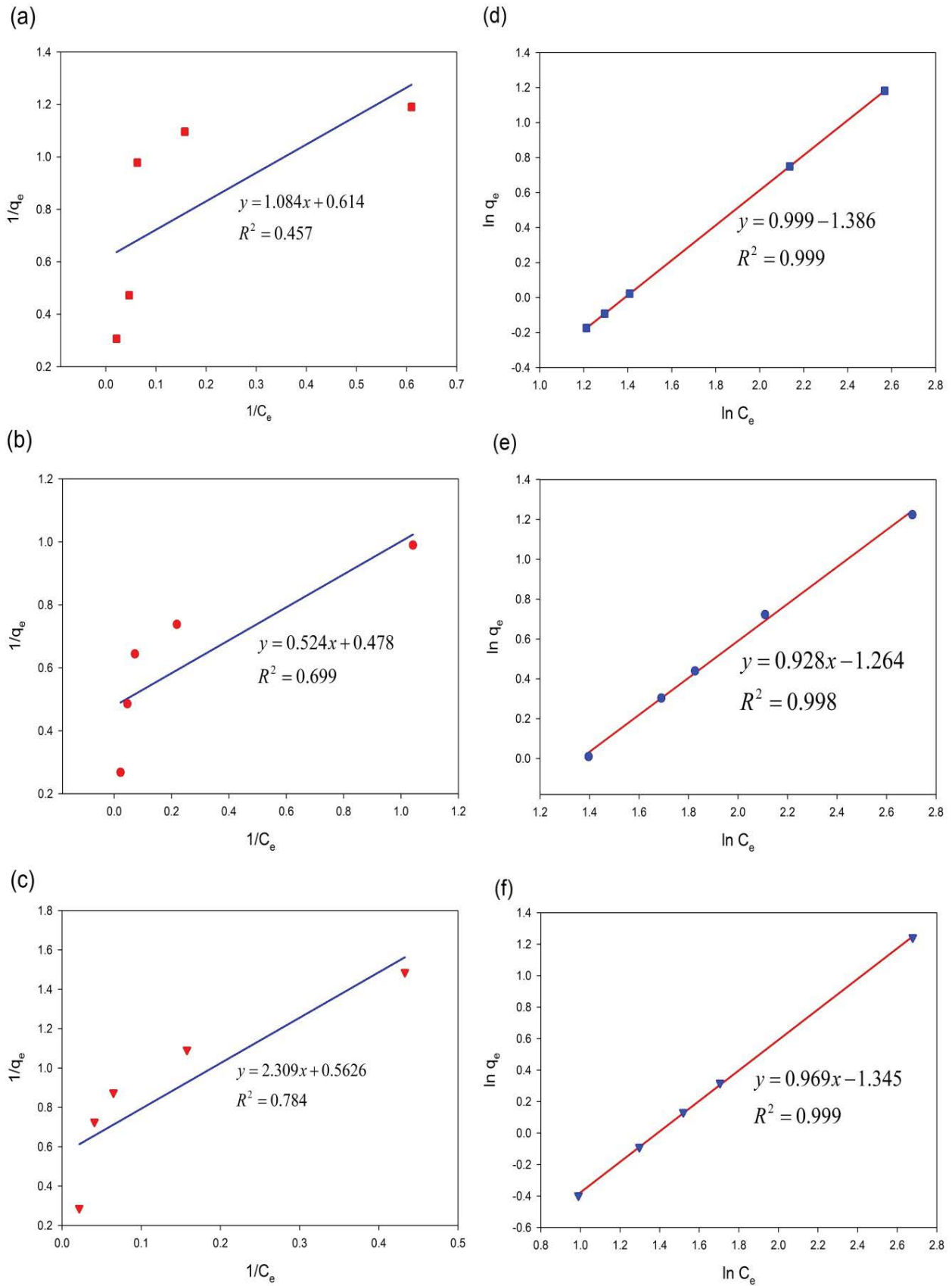


Fig. 6. Langmuir isotherm model (a–c) and Freundlich isotherm model (d–f) for adsorption of Cd²⁺, Pb²⁺, and Ni²⁺ onto CS-Fe/AgNPs.

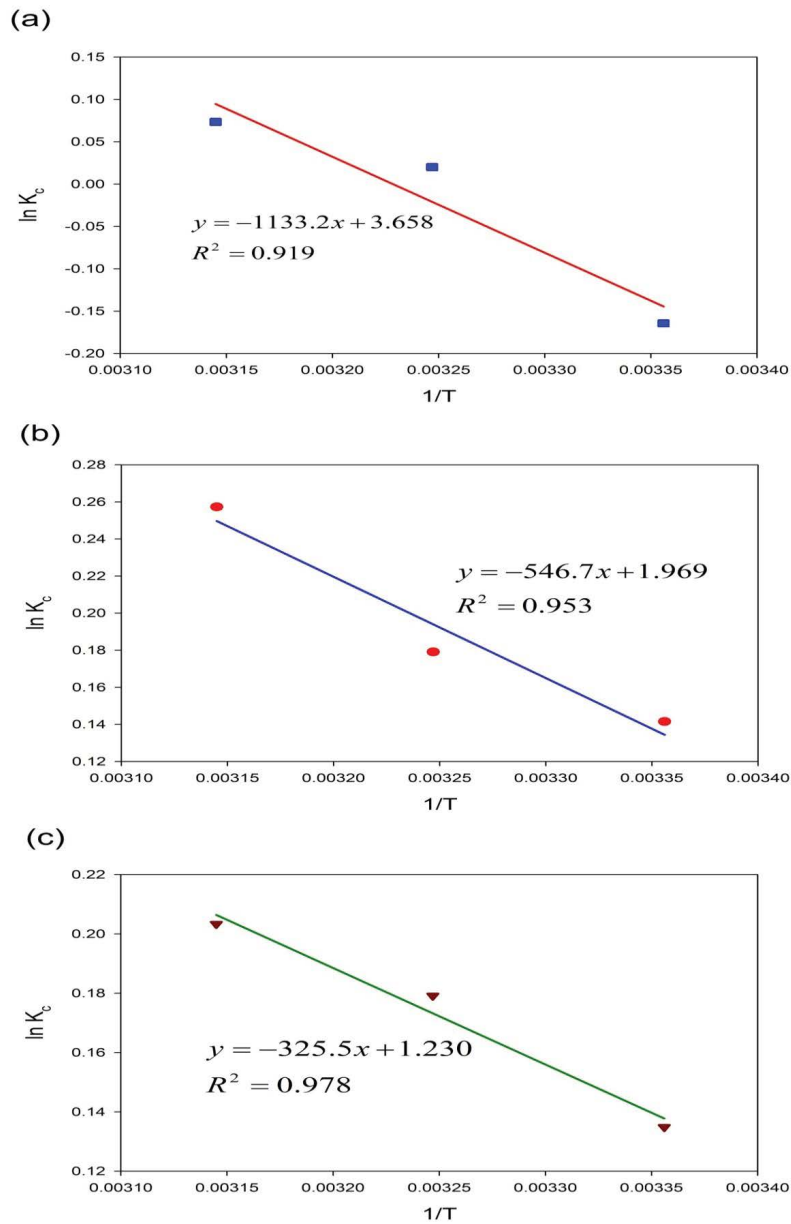


Fig. 7. (a–c) Van't Hoff curve for adsorption of Pb²⁺, Cd²⁺, and Ni²⁺ using CS-Fe/AgNPs.

Table 3
Thermodynamic parameters for Cd²⁺, Pb²⁺, and Ni²⁺ using CS-Fe/AgNPs

Pollutant	T (K)	ΔG° (kJ mol ⁻¹)	ΔH° (kJ mol ⁻¹)	ΔS° (J mol ⁻¹ K ⁻¹)	R ²
Cd ²⁺	298	-407.236	9.42	30.42	0.9188
	308	-51.216	–	–	–
	318	-193.969	–	–	–
Pb ²⁺	298	-350.748	4.54	16.37	0.9527
	308	-458.737	–	–	–
	318	-680.559	–	–	–
Ni ²⁺	298	-334.152	2.71	10.23	0.9908
	308	-458.737	–	–	–
	318	-537.666	–	–	–

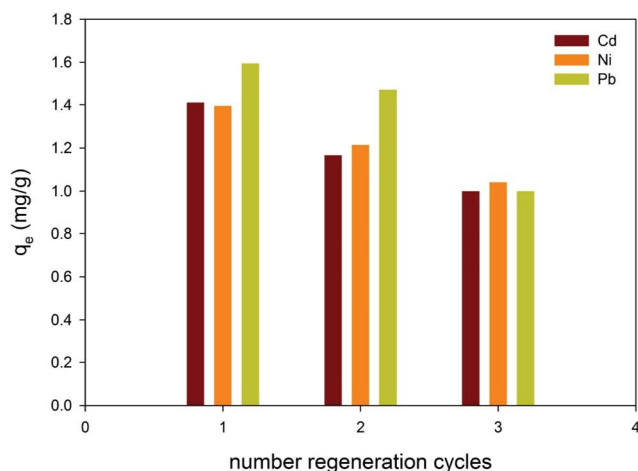


Fig. 8. Regeneration cycles of CS-Fe/AgNPs for the adsorption of Cd²⁺, Pb²⁺, and Ni²⁺ in 0.01 M NaOH solution.

suitability of CS-Fe/AgNPs for only up to two cycles after regeneration.

3.9. Competitive ion adsorption

In this study, the interference of co-existing ion of Cd²⁺, Pb²⁺, and Ni²⁺ was also investigated (results not shown). The composition of industrial or natural wastewater rarely contains single heavy metal and is always a mixture of heavy metals. These heavy metal ions may influence the adsorption of other heavy metal ions and cause interference with one another. The effluent solutions concentrations of each heavy metal ions were fixed at 10 and 20 mg/L with the binding capacities of each heavy metal ion decreases under interference conditions. For the three heavy metal ions adsorption, the affinity order was Pb²⁺ > Cd²⁺ > Ni²⁺ and the ion selectivity of Pb²⁺ was higher due to a larger ionic radius.

4. Conclusion

In this study, a simple chemical method was used to synthesize chitosan (CS), iron/silver bimetallic nanoparticles (Fe/AgNPs), and chitosan-iron/silver bimetallic nanocomposite (CS-Fe/AgNPs). From the XRD pattern, it was seen that the synthesized compound does not have impurity peaks and the respective XRD spectrums specified the production of the individual CS, Fe/AgNPs, and the CS-Fe/AgNPs. The SEM images further indicated that the Fe/AgNPs are spherical shape and of uniform size. The TEM results concluded that the size of the Fe/AgNPs ranges from approximately 10 to 30 nm. This investigation has further illustrated that the CS-Fe/AgNPs showcase functions that make the simultaneous adsorption of Ni²⁺, Cd²⁺, and Pb²⁺ ions possible in model wastewater solutions. The Freundlich isotherm and pseudo-second-order kinetic model fitted well with the adsorption results obtained for Cd²⁺, Pb²⁺, and Ni²⁺ ions. The application of the CS-Fe/AgNPs to adsorption studies demonstrated that it has the potential to remove Pb²⁺, Cd²⁺, and Ni²⁺ ions from wastewater solutions, which should be pursued in future studies.

Acknowledgments

This investigation was sponsored by the National Research Foundation of South Africa and the SensorLab, Chemistry Department at the University of the Western Cape, Bellville in South Africa. A special thanks to the Department of Chemistry, Faculty of Applied Sciences, Cape Peninsula University of Technology, Bellville, South Africa.

References

- [1] A.F. Batisha, Sustainability of water purification based on nanotechnology, *Int. J. Sustainability*, 2 (2013) 12–24.
- [2] M.A. Tofighy, T. Mohammadi, Adsorption of divalent heavy metal ions from water using carbon nanotube sheets, *J. Hazard. Mater.*, 185 (2011) 140–147.
- [3] M. Kumar, H. Furumai, F. Kurisu, I. Kasuga, Potential mobility of heavy metals through coupled application of sequential extraction and isotopic exchange: comparison of leaching tests applied to soil and soak away sediment, *Chemosphere*, 90 (2013) 796–804.
- [4] A. Khan, S. Khan, M.A. Khan, Z. Qamar, M. Waqas, The uptake and bioaccumulation of heavy metals by food plants, their effects on plants nutrients, and associated health risk - a review, *Environ. Sci. Pollut. Res. Int.*, 22 (2015) 13772–13799.
- [5] L.R. Skubal, N.K. Meshkov, T. Rajh, M. Thurnauer, Cadmium removal from water using thiolactic acid-modified titanium dioxide nanoparticles, *J. Photochem. Photobiol., A*, 148 (2002) 393–397.
- [6] S.K. Sharma, *Heavy Metals in Water: Presence, Removal and Safety*, Royal Society of Chemistry, Cambridge, 2015.
- [7] P.B. Tchounwou, C.G. Yedjou, A.K. Patlolla, D.J. Sutton, Heavy metal toxicity and the environment, *EXS*, 101 (2012) 133–164.
- [8] J. An, Q.X. Zhou, W.T. Liu, L.P. Ren, Horizontal distribution and levels of heavy metals in the biggest snowstorm in a century in Shenyang, China, *J. Environ. Sci.*, 20 (2008) 846–851.
- [9] Y. Xi, Y.T. Luo, J.M. Luo, X.B. Luo, Removal of cadmium(II) from wastewater using novel cadmium ion-imprinted polymers, *J. Chem. Eng. Data*, 60 (2015) 3253–3261.
- [10] EPA, The Provision and Quality of Drinking Water in Ireland, A Report for the Year 2008–2009, EPA, 2008, p. 102.
- [11] WHO, Guidelines for Drinking Water Quality, Recommendations, WHO, Geneva, 2008, pp. 317–318.
- [12] NTP, National Toxicology Program, NTP monograph on health effects of low-level lead, *NTP Monogr.*, 13 (2012) 15–148.
- [13] L.F. Chen, H.W. Lang, Y. Lu, C.H. Cui, S.H. Yu, Synthesis of an attapulgite Clay@Carbon nanocomposite adsorbent by a hydrothermal carbonization process and their application in the removal of toxic metal ions from water, *Langmuir*, 27 (2011) 8998–9004.
- [14] S. Luo, T.T. Lu, L. Peng, J.H. Shao, Q.R. Zeng, J.D. Gu, Synthesis of nanoscale zerovalent iron immobilized in alginate microcapsules for removal of Pb(II) from aqueous solution, *J. Mater. Chem. A*, 2 (2014) 15463–15472.
- [15] M. Soylak, A. Kars, I. Narin, Coprecipitation of Ni²⁺, Cd²⁺ and Pb²⁺ for preconcentration in environmental samples prior to flame atomic absorption spectrometric determinations, *J. Hazard. Mater.*, 159 (2008) 435–439.
- [16] M. Ghaedi, Selective and sensitized spectrophotometric determination of trace amounts of Ni(II) ion using α -benzyl dioxime in surfactant media, *Spectrochim. Acta, Part A*, 66 (2007) 295–301.
- [17] G. Bhanjana, N. Dilbaghi, N.K. Singhal, K.-H. Kim, S. Kumar, Copper oxide nanoblades as novel adsorbent material for cadmium removal, *Ceram. Int.*, 43 (2017) 6075–6081.
- [18] X. Weng, S. Lin, Y. Zhong, Z. Chen, Chitosan stabilized bimetallic Fe/Ni nanoparticles used to remove mixed contaminants-amoxicillin and Cd(II) from aqueous solutions, *Chem. Eng. J.*, 229 (2013) 27–34.
- [19] S. Mehdizadeh, S. Sadjadi, S.J. Ahmadi, M. Outokesh, Removal of heavy metals from aqueous solution using platinum

- nanoparticles/Zeolite-4A, *J. Environ. Health Sci. Eng.*, 12 (2014) 7–13, doi: 10.1186/2052-336X-12-7.
- [20] M. Mahmood-ul-Hassan, V. Suthor, E. Rafique, M. Yasin, Removal of Cd, Cr, and Pb from aqueous solution by unmodified and modified agricultural wastes, *Environ. Monit. Assess.*, 187 (2015) 19–26, doi: 10.1007/s10661-014-4258-8.
- [21] F.G.L.M. Borsagli, A.A.P. Mansur, P. Chagas, L.C.A. Oliveira, H.S. Mansu, O-carboxymethyl functionalization of chitosan: complexation and adsorption of Cd(II) and Cr(VI) as heavy metal pollutant ions, *React. Funct. Polym.*, 97 (2015) 37–47.
- [22] I.A. Aguayo-Villarreal, A. Bonilla-Petriciolet, R. Muñiz-Valencia, Preparation of activated carbons from pecan nutshell and their application in the antagonistic adsorption of heavy metal ions, *J. Mol. Liq.*, 230 (2017) 686–695.
- [23] J. Wang, Y. Zhao, P. Zhang, L. Yang, H. Xu, G. Xi, Adsorption characteristics of a novel ceramsite for heavy metals removal from storm water runoff, *Chin. J. Chem. Eng.*, 26 (2018) 96–103.
- [24] G. Sharma, A. Kumar, S. Sharma, M. Naushad, R.P. Dwivedi, Z.A. Alothman, G.T. Mola, Novel development of nanoparticles to bimetallic nanoparticles and their composites: a review, *J. King Saud Univ. Sci.*, 31 (2019) 257–269.
- [25] A.M. Azzam, S.T. El-Wakeel, B.B. Mostafa, M.F. El-Shahat, Removal of Pb, Cd, Cu and Ni from aqueous solution using nano scale zero valent iron particles, *J. Environ. Chem. Eng.*, 4 (2016) 2196–2206.
- [26] C. Jiao, Y. Cheng, W. Fan, J. Li, Synthesis of agar-stabilized nanoscale zero-valent iron particles and removal study of hexavalent chromium, *Int. J. Environ. Sci. Technol.*, 12 (2015) 1603–1612.
- [27] Y. Kuang, J. Du, R. Zhou, Z. Chen, M. Megharaj, R. Naidu, Calcium alginate encapsulated Ni/Fe nanoparticles beads for simultaneous removal of Cu(II) and monochlorobenzene, *J. Colloid Interface Sci.*, 447 (2015) 85–91.
- [28] D.M. Yun, H.H. Cho, J.W. Jang, J.W. Park, Nano zero-valent iron impregnated on titanium dioxide nanotube array film for both oxidation and reduction of methyl orange, *Water Res.*, 47 (2013) 1858–1866.
- [29] Y.S. El-Temsah, E.J. Joner, Effects of nano-sized zero-valent iron (nZVI) on DDT degradation in soil and its toxicity to collembola and ostracods, *Chemosphere*, 92 (2013) 131–137.
- [30] R.K. Singhal, B. Gangadhar, H. Basu, V. Manisha, G.R.K. Naidu, A.V.R. Reddy, Remediation of malathion contaminated soil using zero valent iron nanoparticles, *Am. J. Anal. Chem.*, 3 (2012) 76–82.
- [31] B. Geng, Z.H. Jin, T.L. Li, X.H. Qi, Preparation of chitosan-stabilized Fe⁰ nanoparticles for removal of hexavalent chromium in water, *Sci. Total Environ.*, 407 (2009) 4994–5000.
- [32] T. Liu, X. Yang, Z.-L. Wang, X. Yan, Enhanced chitosan beads-supported Fe⁰-nanoparticles for removal of heavy metals from electroplating wastewater in permeable reactive barriers, *Water Res.*, 47 (2013) 6691–6700.
- [33] T. Phenrat, N. Saleh, K. Sirk, R.D. Tilton, G.V. Lowry, Aggregation and sedimentation of aqueous nanoscale zerovalent iron dispersions, *Environ. Sci. Technol.*, 41 (2007) 284–290.
- [34] L. Wu, J.P. She, T.Q. Zhao, Q.Q. Wang, L.L. Xu, Comparative study on degradation of methyl orange by resin-supported nano-iron and nano-iron/nickel, *Acta Sci. Circum.*, 33 (2013) 1585–1589.
- [35] Z.T. Liu, C.G. Gu, M. Ye, Y.R. Bian, Y.W. Cheng, F. Wang, X.L. Yang, Y. Song, X. Jiang, Debromination of polybrominated diphenyl ethers by attapulgite supported Fe/Ni bimetallic nanoparticles: influencing factors, kinetics and mechanism, *J. Hazard. Mater.*, 298 (2015) 328–337.
- [36] Y. Li, Y. Xiao, X.Q. Li, C. Chen, Degradation of phenanthrene by nanoscale zerovalent iron and its bimetallic nanoparticles, *Acta Sci. Circum.*, 35 (2015) 499–507.
- [37] G.N. Jovanovic, J.E. Atwater, Z.P. Polona, I. Plazl, Dechlorination of polychlorinated phenols on bimetallic Pd/Fe catalyst in a magnetically stabilized fluidized bed, *Chem. Eng. J.*, 274 (2015) 50–60.
- [38] C. van der Horst, V. Somerset, Technologies for Remediation of Emerging Contaminants in Wastewater Samples, E. Fosso-Kankeu, Ed., *Nano and Bio-Based Technologies for Wastewater Treatment*, John Wiley & Sons, Inc., Hoboken, NJ, USA, 2019, pp. 429–458.
- [39] C. van der Horst, B. Silwana, E. Iwuoha, V. Somerset, Synthesis and characterisation of bismuth–silver bimetallic nanoparticles for electrochemical sensor applications, *Anal. Lett.*, 48 (2015) 1–22.
- [40] E. Roy, S. Patra, A. Tiwari, R. Madhuri, P.K. Sharma, Single cell imprinting on the surface of Ag–ZnO bimetallic nanoparticle modified graphene oxide sheets for targeted detection, removal and photothermal killing of *E. coli*, *Biosens. Bioelectron.*, 89 (2017) 620–626.
- [41] H. Wu, Q. Feng, Fabrication of bimetallic Ag/Fe immobilized on modified biochar for removal of carbon tetrachloride, *J. Environ. Sci.*, 54 (2017) 346–357.
- [42] Y. Ma, X. Wu, G. Zhang, Core-shell Ag@Pt nanoparticles supported on sepiolite nanofibers for the catalytic reduction of nitrophenols in water: enhanced catalytic performance and DFT study, *Appl. Catal., B*, 205 (2017) 262–270.
- [43] X. Wang, F. Li, J. Yang, Polyvinyl pyrrolidone-modified Pd/Fe nanoparticles for enhanced dechlorination of 2,4-dichlorophenol, *Desal. Water Treat.*, 52 (2014) 7925–7936.
- [44] Y. Shen, L. Li, Z. Zhang, Scalable and environmentally friendly synthesis of hierarchical magnetic carbon nanosheet assemblies and their application in water treatment, *J. Phys. Chem. C*, 120 (2016) 6659–6668.
- [45] B. Kakavandi, R.R. Kalantary, M. Farzadkia, A.H. Mahvi, A. Esrafil, A. Azari, A.R. Yari, A.B. Javid, Enhanced chromium(VI) removal using activated carbon modified by zero valent iron and silver bimetallic nanoparticles, *J. Environ. Health Sci. Eng.*, 15 (2014) 115–124.
- [46] V. Zamora-Mora, M. Fernández-Gutiérrez, Á. González-Gómez, B. Sanz, J.S. Román, G.F. Goya, R. Hernández, C. Mijangos, Chitosan nanoparticles for combined drug delivery and magnetic hyperthermia: from preparation to *in vitro* studies, *Carbohydr. Polym.*, 157 (2017) 361–370.
- [47] U. Soni, J. Bajpai, S. Kumar Singh, A.K. Bajpai, Evaluation of chitosan-carbon based biocomposite for efficient removal of phenols from aqueous solutions, *J. Water Process Eng.*, 16 (2017) 56–63.
- [48] V. Sureshkumar, S.C.G. Kiruba Daniel, K. Ruckmani, M. Sivakumar, Fabrication of chitosan–magnetite nanocomposite strips for chromium removal, *Appl. Nanosci.*, 6 (2016) 277–285.
- [49] R. Yuvakkumar, V. Elango, V. Rajendran, N. Kannan, Preparation and characterization of zero valent iron nanoparticles, *Dig. J. Nanomater. Biostruct.*, 6 (2011) 1771–1776.
- [50] J.O. Marques Neto, C.R. Bellato, J.L. Milagres, K.D. Pessoa, E.S. De Alvarenga, Preparation and evaluation of chitosan beads immobilized with iron(III) for the removal of As(III) and As(V) from water, *J. Braz. Chem. Soc.*, 24 (2013) 121–132.
- [51] B. Silwana, C. van der Horst, E. Iwuoha, V. Somerset, Synthesis, characterisation and electrochemical evaluation of reduced graphene oxide modified antimony nanoparticles, *Thin Solid Films*, 592 (2015) 124–134.
- [52] V. Somerset, C. Van der Horst, B. Silwana, C. Walters, E. Iwuoha, Biomonitoring and evaluation of metal concentrations in sediment and crab samples from the north-west province of South Africa, *Water Air Soil Pollut.*, 226 (2015) 43–67, doi: 10.1007/s11270-015-2329-2.
- [53] M.A. Correa-Duarte, M. Giersig, N.A. Kotov, L.M. Liz-Marzan, Control of packing order of self-assembled monolayers of magnetite nanoparticles with and without SiO₂ coating by microwave irradiation, *Langmuir*, 14 (1998) 6430–6435.
- [54] G. Saraswathy, S. Pal, C. Rose, T.P. Sastry, A novel bio-inorganic bone implant containing deguel bone, chitosan and gelatin, *Bull. Mater. Sci.*, 24 (2001) 415–420.
- [55] S. Mekahlia, B.B. Ouzid, Chitosan-copper(II) complex as antibacterial agent: synthesis, characterization and coordinating bond-activity correlation study, *Phys. Procedia*, 2 (2009) 1045–1053.
- [56] A. Azari, H. Gharibi, B. Kakavandi, G. Ghanizadeh, A. Javid, A.H. Mahvi, K. Sharafi, T. Khosravia, Magnetic adsorption

- separation process: an alternative method of mercury extracting from aqueous solution using modified chitosan coated Fe_3O_4 nanocomposites, *J. Chem. Technol. Biotechnol.*, 92 (2017) 188–200.
- [57] S. Wazed Ali, S. Rajendran, M. Josh, Synthesis and characterization of chitosan and silver loaded chitosan nanoparticles for bioactive polyester, *Carbohydr. Polym.*, 83 (2001) 438–446.
- [58] K.V.H. Prashanth, F.S. Kittur, R.N. Tharanathan, Solid state structure of chitosan prepared under different N-deacetylating conditions, *Carbohydr. Polym.*, 50 (2002) 27–33.
- [59] L. Kong, Y. Gao, W. Cao, Y. Gong, N. Zhao, X. Zhang, Preparation and characterization of nano-hydroxyapatite/chitosan composite, *J. Biomed. Mater. Res. Part A*, 75 (2005) 275–282.
- [60] X. Wang, Y. Du, H. Liu, Preparation, characterization and antimicrobial activity of chitosan–Zn complex, *Carbohydr. Polym.*, 56 (2004) 21–26.
- [61] J.-W. Rhim, S.-I. Hong, H.-M. Park, K.W. Perry, Preparation and characterization of chitosan-based nanocomposite films with antimicrobial activity, *J. Agric. Food Chem.*, 54 (2006) 5814–5822.
- [62] M.H. Rashid, T.K. Mandal, Synthesis and catalytic application of nanostructured silver dendrites, *J. Phys. Chem. C*, 111 (2007) 16750–16760.
- [63] X.Y. Wang, C. Chen, H.L. Liu, J. Ma, Characterization and evaluation of catalytic dechlorination activity of Pd/Fe bimetallic nanoparticles, *Ind. Eng. Chem. Res.*, 47 (2008) 8645–8651.
- [64] S. Shahabuddin, N.M. Sarih, F.H. Ismail, M.M. Shahid, N.M. Huang, Synthesis of chitosan grafted polyaniline/ Co_3O_4 nanocube nanocomposites and their photocatalytic activity toward methylene blue dye degradation, *RSC Adv.*, 5 (2015) 83857–83867.
- [65] H.-H. Cho, K. Wepasnick, B.A. Smith, F.K. Bangash, D.H. Fairbrother, W.P. Ball, Sorption of aqueous Zn(II) and Cd(II) by multiwall carbon nanotubes: the relative roles of oxygen-containing functional groups and graphenic carbon, *Langmuir*, 26 (2009) 967–981.
- [66] C.P.J. Isaac, A. Sivakumar, Removal of lead and cadmium ions from water using *Annona squamosa* shell: kinetic and equilibrium studies, *Desal. Water Treat.*, 51 (2013) 7700–7709.
- [67] C. Obi, O.E. Njoku, Removal of Ni(II) and Pb(II) ions from aqueous solutions by grapefruit (*Citrus paradisi*) mesocarp biomass, *J. Appl. Sci. Environ. Manage.*, 19 (2015) 536–444.
- [68] K.S. Low, C.K. Lee, K.P. Lee, Sorption of copper by dye-treated oil-palm fibres, *Bioresour. Technol.*, 44 (1993) 109–112.
- [69] G.O. El-Sayed, H.A. Dessouki, S.S. Ibrahim, Removal of Zn(II), Cd(II) and Mn(II) from Aqueous solutions by adsorption on maize stalks, *Malaysian J. Anal. Sci.*, 15 (2011) 8–21.
- [70] N. Mansouriieh, M.R. Sohrabi, M. Khosravi, Adsorption kinetics and thermodynamics of organophosphorus profenofos pesticide onto Fe/Ni bimetallic nanoparticles, *Int. J. Environ. Sci. Technol.*, 13 (2016) 1393–1404.
- [71] R. Sahraei, M. Ghaemy, Synthesis of modified gum tragacanth/graphene oxide composite hydrogel for heavy metal ions removal and preparation of silver nanocomposite for antibacterial activity, *Carbohydr. Polym.*, 157 (2017) 823–833.
- [72] Y. Bulut Y, Z. Tez, Removal of heavy metals from aqueous solution by sawdust adsorption, *J. Environ. Sci.*, 19 (2007) 160–166.
- [73] Z.S. Pour, M. Ghaemy, Removal of dyes and heavy metal ions from water by magnetic hydrogel beads based on poly(vinyl alcohol)/carboxymethylstarch-g-poly(vinyl imidazole), *RSC Adv.*, 5 (2015) 64106–64118.
- [74] R. Khandanlou, M.B. Ahmad, H.R. Fard Masoumi, K. Shamel, M. Basri, K. Kalantari, Rapid adsorption of copper(II) and lead(II) by rice straw/ Fe_3O_4 nanocomposite: optimization, equilibrium isotherms, and adsorption kinetics study, *PLoS One*, 10 (2015) 1–19.
- [75] R.K. Gautam, P.K. Gautam, S. Banerjee, S. Soni, S.K. Singh, M.C. Chattopadhyaya, Removal of Ni(II) by magnetic nanoparticles, *J. Mol. Liq.*, 204 (2015) 60–69.
- [76] G.M. Walker, L.R. Weatherley, Adsorption of dyes from aqueous solution - the effect of adsorbent pore size distribution and dye aggregation, *Chem. Eng. J.*, 83 (2001) 201–206.
- [77] H.K. Boparai, M. Joseph, D.M. O'Carroll, Kinetics and thermodynamics of cadmium ion removal by adsorption onto nano zerovalent iron particles, *J. Hazard. Mater.*, 186 (2011) 458–465.
- [78] L.P. Lingamdinne, H. Roh, Y.L. Choi, J.R. Koduru, J.K. Yang, Y.Y. Chang, Influencing factors on sorption of TNT and RDX using rice husk biochar, *J. Ind. Eng. Chem.*, 32 (2015) 178–186.
- [79] T. Wang, J. Lin, Z. Chen, M. Megharaj, R. Naidu, Green synthesized iron nanoparticles by green tea and eucalyptus leaves extracts used for removal of nitrate in aqueous solutions, *J. Cleaner Prod.*, 83 (2014) 413–419.
- [80] L. Fan, Y. Zhang, X. Li, C. Luo, F. Lu, H. Qiu, Removal of alizarin red from water environment using magnetic chitosan with alizarin red as imprinted molecules, *Colloids Surf., B*, 91 (2012) 250–257.